Available online at www.sciencedirect.com

ScienceDirect

Geochimica et Cosmochimica Acta 284 (2020) 254–272

Geochimica et Cosmochimica Acta

www.elsevier.com/locate/gca

Conservation of oxygen and hydrogen seasonal isotopic signals in meteoric precipitation in groundwater: An experimental tank study of the effects of land cover in a summer monsoon climate

Yundi Hu [a,b,d], Zaihua Liu [a,c,d,*], Derek Ford [e,*], Min Zhao [a,d], Qian Bao [a,d,f], Cheng Zeng [a,d], Xiaoyu Gong [a,d,f], Yu Wei [a,f], Xianli Cai [a,d,f], Jia Chen [a,d,f]

[a] State Key Laboratory of Environmental Geochemistry, Institute of Geochemistry, CAS, Guiyang 550081, Guizhou, China
[b] School of Geography and Environmental Science, Guizhou Normal University, Guiyang 550025, Guizhou, China
[c] CAS Center for Excellence in Quaternary Science and Global Change, 710061 Xi'an, China
[d] Puding Karst Ecosystem Research Station, Chinese Ecosystem Research Network, Chinese Academy of Sciences, Puding 562100, Guizhou, China
[e] School of Geography and Earth Science, McMaster University, Hamilton, ON L8S 4K1, Canada
[f] University of Chinese Academy of Sciences, Beijing 100049, China

Received 6 March 2020; accepted in revised form 29 June 2020; available online 7 July 2020

Abstract

$\delta^{18}O$ and δD values in meteoric groundwaters reflect those in their source precipitation, which normally displays seasonal ranges of several to many permil. Normally there are substantial reductions in the groundwater isotopic ranges due to mixing in any vegetation, soil cover and the aquifer itself, plus the distortions that can be introduced by evaporation. Nevertheless, in carbonate karst regions (and others) many spring waters are found to preserve significant proportions of these seasonal signals. They are of current interest because they may also be detected in calcite speleothems precipitated from groundwater in caves, in calcretes and calcareous nodules in soils, etc. thus permitting detailed paleoclimate reconstructions.

This paper presents some baseline data on reduction of isotope seasonal signals in groundwater that are pertinent to such speleothem studies. They are from artificial tank experiments at Shawan Karst Test Site, Guizhou, China. The climate is humid subtropical with mean annual precipitation of 1340 mm, >80% falling between May and October. The concrete tanks measure 20 × 5 m, 3 m deep each, point-drained at one end to simulate a spring. They are filled with 2.5 m of local limestone quarry gravel, creating carbonate aquifers with primary porosities ~ 50%. A first tank is left bare, simulating the rocky desertification found in parts of the region. The other tanks are topped with 0.5 m of local, clay-rich residual soil, one left bare, the other three sown with rainy season corn, permanent grass and permanent shrubs respectively. Measurements cover the three climatic years, November 2015-November 2018. > 90% of the rainfall events were sampled, and the drains every ten days.

$\delta^{18}O$ and δD in the rainfall displayed strong and regular sinusoidal oscillations with the successive seasons. In the bare rock tank these were reduced (damped) by 56~74% in the different years, with phase (time) lags of 127~134 days at the drain. In the soil-topped tanks damping ranged from 61% to 93% and the time lags from 164 to 202 days: differences between them are not statistically significant but all do differ significantly from the bare rock. In all cases, the responses of the two isotopes were similar in direction and magnitude. The 0.5 m soil cover had the most important effect. The bare rock aquifer conserved the most information. Losses were similar in the four soil-topped tanks, responding to stronger evaporation and obstruction

* Corresponding authors at: State Key Laboratory of Environmental Geochemistry, Institute of Geochemistry, CAS, Guiyang 550081, Guizhou, China (Z. Liu). School of Geography and Earth Science, McMaster University, Hamilton, ON L8S 4K1, Canada (D. Ford).
E-mail addresses: liuzaihua@vip.gyig.ac.cn (Z. Liu), dford@mcmaster.ca (D. Ford).

https://doi.org/10.1016/j.gca.2020.06.032

of flow in the soil. These findings are briefly compared to seasonal isotope variations reported in speleothem drip waters in limestone caves in China and elsewhere in the world.

Keywords: Groundwater; Precipitation; Oxygen and hydrogen isotope; Land cover; Phase lag time; Damping effect; Isotopic seasonality

1. INTRODUCTION

Since the 1950s and 1960s, stable oxygen and hydrogen isotope ratios ($\delta^{18}O$ and δD) have been widely used as important tools in studies of the hydrological cycle because, being the components of water molecules, they are optimal natural tracers (Dansgaard, 1953; Craig, 1961; Kendall and McDonnell, 2012; Mueller et al., 2014; Jones et al., 2016; Zhao et al., 2018). $^{18}O/^{16}O$ ratios in calcite speleothems, now a commonly used proxy for studying past climate change, are dominated primarily by the isotopic composition of the feed water, which is normally groundwater in the unsaturated (vadose) zone. Up to now, most studies have focused on $\delta^{18}O$ speleothem records over long time scales, achieving many breakthroughs in paleoclimate study (McDermott et al., 2001; Yadava et al., 2004; Wang et al., 2005; Sinha et al., 2019), while less attention has been paid to the short time scales that may also contain much significant high-resolution information (Fairchild et al., 2006; Fairchild and Baker, 2012). As the development of analytical techniques has progressed, speleothem isotopic data at short time scales, e.g. annual or seasonal, can be now obtained (Kolodny et al., 2003; Treble et al., 2005; Frappier et al., 2007). Unlocking the information preserved in them is likely to be a focus of much future research. However, many speleothems will also register unique local variations caused by the biophysical environment on the open surface above them, in the soil and in any epikarst present (Serefiddin et al., 2004; Soubiès et al., 2005; Belli et al., 2013). To better understand variations in speleothem records at these more subtle and shorter time scales requires quantitative investigation of the local factors affecting oxygen and hydrogen isotopic fractionation of the infiltrating water.

When precipitation infiltrates through the complex sequence of vegetation-litter-soil-epikarst (if present)-bedrock to recharge a groundwater aquifer, it is commonly accompanied by damping and time lag of seasonal variations in $\delta^{18}O$ and δD. In a pioneer transect of speleothem drip sites in many caves between Texas (Lat. 35°N) and upstate New York (45°N) Yonge et al. (1985) found a close match with the global Craig-Dansgaard Line and little or no seasonal isotopic variation. In China, Luo et al. (2014) reported minor seasonal variation of $\delta^{18}O$ in two drips in Guizhou. Duan et al. (2016) studied the $\delta^{18}O$ of 34 drips from eight caves in eight provinces, finding that only 18% of drips had seasonal variation. In contrast, Beddows et al. (2016) reported $\delta^{18}O$ damped an average 73% over three sampling years at nine drip sites in shallow caves at different elevations on the humid west coast of British Columbia. To promote the study of $\delta^{18}O$ speleothem records over short time scales, therefore, several successive years of data from controlled (i.e. experimental) sites that display well-preserved seasonality are desirable. Further, determining the time lags is essential to establish the correct correlations between given rainfall inputs and their groundwater outputs at drips or springs. It is often difficult to calculate these lag times, but they may be estimated by phase shifts in the isotopes or by the amplitude of groundwater isotopic seasonality compared to that in the precipitation (A/A_0) (Maloszewski et al., 1983; Reddy et al., 2006; Beddows et al., 2016; Kirchner, 2016). The former is generally less precise, while the latter involves many assumptions (e.g. about evaporation): thus, studies of lag times in speleothems may be improved by controlled experiments in model karst groundwaters.

Previous studies have found that the damping of the seasonal isotopic variations in precipitation is chiefly determined by the hydrodynamic conditions, length of the flow path, and isotopic composition of any previous water available for mixing in the aquifer (Eichinger et al., 1984; Clark and Fritz, 1997; Bradley et al., 2010; Luo et al., 2014). In isotopic studies of soil water generally, the deeper the soil, the greater is the damping (Eichinger et al., 1984; Tang and Feng, 2001; Comas-Bru and McDermott, 2015). From isotopic theory, the composition of any prior water in an aquifer is affected chiefly by its evaporation history and water–rock interactions (Clark and Fritz, 1997; Wackerbarth et al., 2012; Beddows et al., 2016). For example, Markowska et al. (2016) found that some drip waters that had experienced evaporation were enriched up to 3‰ $\delta^{18}O$ compared to the precipitation. Generally, the damping of seasonal isotopic variations in precipitation will be influenced by a complex of factors in the overlying vegetation, soil and in the karst aquifer. Many studies have shown that the type of land cover is a dominant control of the hydrodynamic conditions and amounts of evaporation (e.g. Zhang et al., 2001; Raymond et al., 2008; Zhao et al., 2018). Raymond et al. (2008) found that the percentage of cropland cover greatly influenced the discharge of precipitation. Similarly, Zeng et al (2016) reported that catchments with dense vegetation will reduce the recharge coefficient of precipitation. Zhao et al. (2018) have shown the evaporation losses of shrub lands were higher than in evergreen forests. Given the complexity of the vegetation, soil, bedrocks, and of delimiting catchments in natural karst watersheds, there have been few systematic studies of the effects of single land cover types (vegetation plus soil) on seasonal patterns of $\delta^{18}O$ and δD in the groundwaters beneath them. We have established the Shawan Karst Test Site, Guizhou, China, to model five types of watersheds and aquifers. They are of identical size, with identical bedrocks and boundaries but different land covers - a bare rock surface, bare soil surface, cropped surface, grassland, and

shrubbery; see the details in Section 2. In previous studies at the Test Site, we have shown that the strengths of evaporation and groundwater discharge are highly affected by the type of land cover (Hu et al., 2018). In this study we chiefly discuss the effects of differing land cover on reduction of isotope seasonal signals of rainfall, revealing their impacts on the conservation of precipitation isotopic variation in the groundwaters at seasonal and annual timescales.

2. THE STUDY SITE

The Shawan Karst Test Site is located within the Puding Comprehensive Karst Research and Experimental Station (26°14′-26°15′N, 105°42′-105°43′E, 1200 m), Guizhou Province, Southwest China (Fig. 1a). This area experiences a typical humid subtropical monsoonal climate. From the China Meteorological Data Network, for the 30 years period 1981–2010, Puding had a mean annual air temperature of 15.2 °C, mean annual precipitation of 1341 mm, and mean annual relative humidity of 78%. Precipitation is concentrated in the rainy season, May to October, when more than 80% of the annual total falls, accompanied by higher temperatures than in the dry season (Zhao et al., 2010; Yang et al., 2012). There is a meteorological station installed at the Puding Station (Fig. 1c) that is within 100 m of the Shawan Test Site and provides daily precipitation, air temperature, relative humidity data, etc.

As noted, the test site is built to simulate natural watersheds, with identical hydrogeological conditions (bedrocks and watershed boundaries) but different land covers. It consists of five adjoining concrete tanks (Fig. 1b), each 20 m in length, 5 m wide and 3 m deep. In order to create an impervious boundary, each tank is coated with epoxy resin and covered with HDPE film that is stable and generally will not react with groundwater. All tanks are filled with 2.5 m of dolomitic limestone gravel from the local Guanling Formation (Middle Triassic), to serve as a granular (or 'matrix') aquifer that has karstic water chemistry. The limestone was from a local quarry and machine-ground into angular clasts with grain sizes ranging 0.5 cm to 6 cm. Porosity is about 0.5 (Zhu et al., 2015). There is no soil and vegetation cover in the first tank – just bare rock

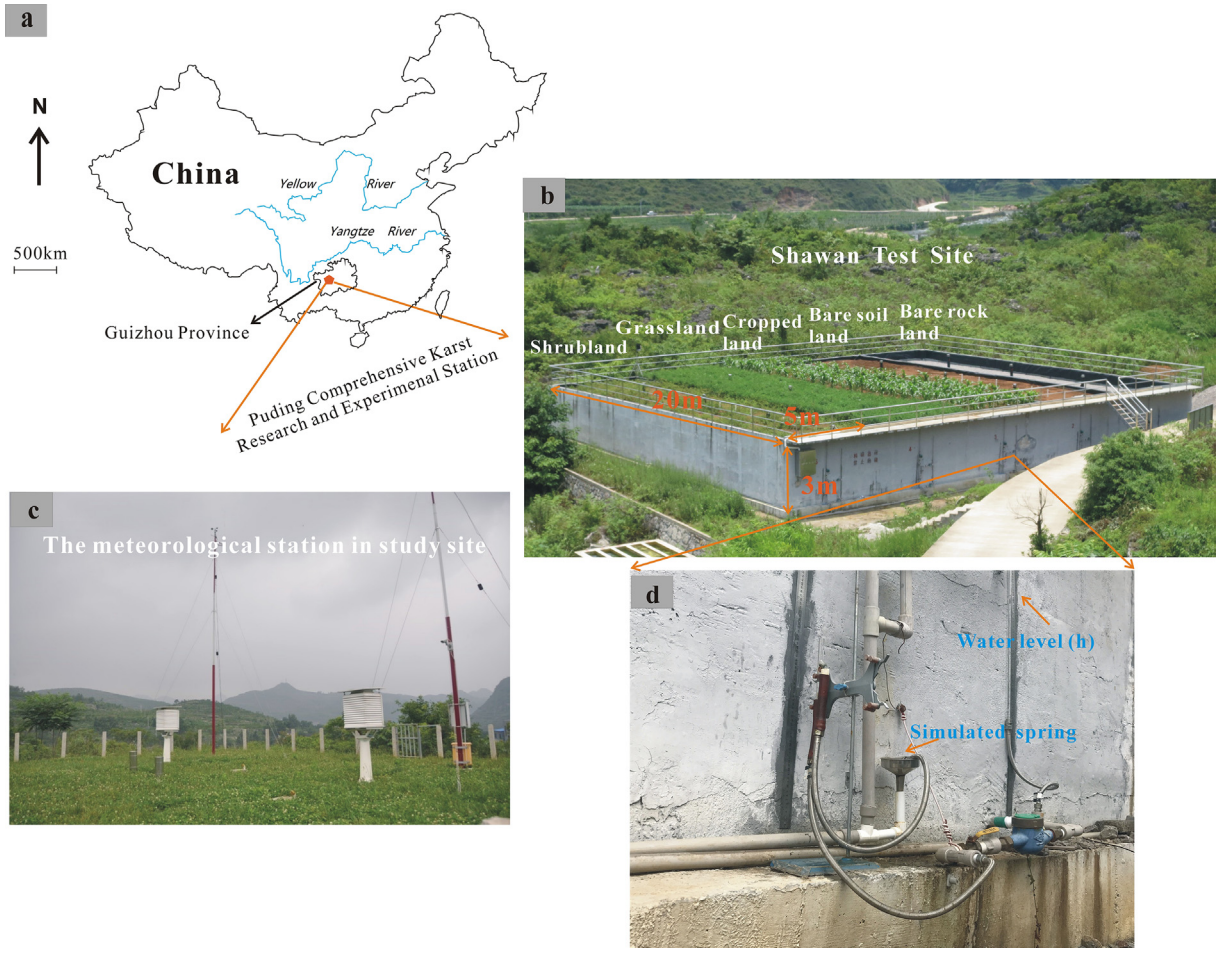

Fig. 1. (a) The location of Puding Comprehensive Karst Research and Experimental Station (26°14′-26°15′N, 105°42′-105°43′E, 1200 m) in Guizhou Province, Southwest China. (b) The Shawan Test Site consists of five concrete tanks that simulate watersheds with different land covers: bare rock (coarse gravel), bare soil, cropped land (corn), grassland (alfalfa), and shrubland (Roxburgh roses). (c) The meteorological station at the study site is within 100 m of the Shawan Test Site. (d) The simulated spring and device for measuring water levels in each tank.

Table 1
Chemical compositions of rock and soil samples from the Shawan Test Site. (From Zeng et al., 2017).

Chemicals	Al_2O_3	BaO	CaO	Cr_2O_3	TFe_2O_3	K_2O	MgO	MnO	Na_2O	P_2O_5	SiO_2	SrO	TiO_2	LOI [a.]	Total
	(%)														
Rock	0.51	0.02	46.15	<0.01	0.31	0.22	7.40	<0.01	0.03	0.01	1.42	0.08	0.04	44.03	100.19
Soil	22.04	0.02	0.64	0.02	9.70	0.85	1.60	0.32	0.10	0.24	49.31	0.01	1.48	12.68	99.01

[a.] LOI: Loss On Ignition at 1,000 °C.

(gravel surface) to simulate karst areas with an extreme degree of rocky desertification. The other four tanks are covered by 0.5 m of clay-rich residual soil from a local field underlain by the same Guanling dolomitic limestone: see Table 1 and Zeng et al. (2017) for details of the chemical composition of the rock and soil materials. The second tank has only soil and no vegetation, simulating bare soil conditions. The remaining three tanks are planted with corn, alfalfa and Roxburgh roses respectively, to simulate regularly cropped land, perennial grasslands and shrub lands. The corn is only present during its growing season from May to August. The alfalfa and Roxburgh roses were sown in January 2014 and left undisturbed. More details can be found in Zeng and Liu (2013), Chen et al. (2017) and Zeng et al. (2017). A drainage outlet with an internal diameter of about 2 mm in each tank simulates a permanent karst spring issuing from a matrix aquifer, and an adjoining piezometer measures groundwater water levels (Fig. 1d). Each tank thus functions as a small but complete watershed with a primary aquifer of coarse dolomitic limestone gravel, a controlled boundary and single kind of land cover (vegetation and soil). They are independent groundwater systems that are recharged only by the natural rainfall, by infiltration through vegetation, soil and bedrock, and discharged at the artificial springs.

3. METHODS

3.1. Sampling and analysis

Daily meteorological data were recorded from November 2015 to November 2018 at the study site. Based on IAEA/GNIP guidelines for precipitation sampling, a total of 274 rainfall samples, encompassing more than 90% of the precipitation events that occurred during the three years, were collected by standard gauges for the isotopic measurements. The rainwater was removed from the collectors and passed through 0.45 μm Millipore filters into 20 ml high-density polyethylene bottles soon after each rainfall event, in order to prevent evaporation. To obtain high resolution data on the groundwater isotopic and hydrological responses, each simulated spring was sampled on the same day at ten day intervals. Groundwater discharges and water levels were also measured during the sampling. Discharge data were determined by volumetric cylinder and stopwatch. As with the rainfall, groundwater samples were passed through 0.45 μm Millipore filters into 20 ml high-density polyethylene bottles. Finally, all samples were sealed with Parafilm and stored in a refrigerator at ~ 4 °C.

The precipitation and groundwater samples were analyzed for $\delta^{18}O$ and δD at the State Key Laboratory of Environmental Geochemistry, Institute of Geochemistry, Chinese Academy of Sciences, with a Los Gatos Research DLT-100 liquid isotope water analyzer, using the methods described in Lis et al. (2008). Before testing, samples were taken out of the refrigerator at least two hours in advance to bring their temperature into equilibrium with room temperature. The standard deviation (1σ) of measurement was ± 0.1‰ for $\delta^{18}O$ and ± 0.5‰ for δD. All standards and measured values are reported against Vienna-Standard Mean Ocean Water (V-SMOW).

3.2. Statistical analysis

3.2.1. Phase lag time estimation

The seasonal variations of $\delta^{18}O$ and δD in the precipitation at Puding can be approximated as simple sine curves, which are expected to be dampened and shifted during the processes of infiltration and recharge of the aquifer. As long as the sinusoidal variations of $\delta^{18}O$ and δD in the groundwater are not completely damped, the amplitude differences and phase shifts between precipitation and groundwater can be used to estimate the lag time, i.e. groundwater mean residence time (MRT) between the precipitation event and discharge at the spring (Clark and Fritz, 1997). The seasonal variations in $\delta^{18}O$ and δD tend to follow the sine function:

$$\delta = I + A\sin[(2\pi t/b) + c] \quad (1)$$

where δ is the isotopic composition of precipitation and groundwater ($\delta^{18}O$ and δD), I is the sine offset on the δ axis which can roughly represent the annual mean δ, A is the seasonal amplitude of the sine function (the difference between the maximum and minimum values of the sine curve divided by 2), b is the period of the sinusoidal cycle which is taken to be 365 days, t is time in days, and c is the phase lag in radians (Maloszewski et al., 1983; Stewart and McDonnell, 1991; Reddy et al., 2006). These parameters can be determined by sinusoidal regression analysis. To avoid extra calculation, we constrained the range of c from -2π to 2π.

Given the impact of evaporation on the seasonal amplitudes of $\delta^{18}O$ and δD in the watersheds, in this study we use the phase lag to calculate groundwater lag time instead of using the seasonal amplitude. We assign t_0 as the time of the sine peak. According to the fitted c results in Eq. (1), the value of n can be determined by Eqs. (2) and (3). Note that the variable n is a dimensionless constant, which is used to coordinate peak value of sinusoidal cycle.

$$-2\pi < c < \pi/2 \; n = 0 \quad (2)$$

$$\pi/2 < c < 2\pi \; n = 1 \quad (3)$$

When the value of n is determined, the peak value of $\pi/2$ or $5\pi/2$ can be determined and the t_0 of precipitation and groundwater reaching their sine peaks obtained (Eq. (4)). Thus, the phase lag time between precipitation and groundwater ($\triangle$t) can be calculated through Eq. (5). It should be noted that this method assumes that the phase lag between precipitation and groundwater does not exceed one sinusoidal cycle; i.e. the calculated result is less than one year in duration (Beddows et al., 2016).

$$(2\pi t_0/b) + c = \pi/2 + 2n\pi, \quad (4)$$

$$\Delta t = t_0(\text{groundwater}) - t_0(\text{precipitation}) \quad (5)$$

3.2.2. Statistical testing

Given that the groundwater in the five simulated watersheds all derives from the same precipitation events, we set up the null hypotheses that $\delta^{18}O$ and δD of the groundwater in them are not significantly different from one another and from that of the precipitation. To assess whether there are statistically significant differences of mean and variance between them, Student's t-test and F-test were applied respectively.

4. RESULTS

4.1. Hydrometeorological data

The basic meteorological and hydrological data - air temperature, precipitation, groundwater levels, groundwater discharges, above and in the different tanks from November 2015 to November 2018 are plotted in Fig. 2. All of them display clear seasonal variations. Air temperature and precipitation are higher in the rainy season than in the dry, precipitation being sharply concentrated in a characteristic subtropical monsoon regime (Fig. 2a). It is seen that both the five water levels and discharges had similar seasonal patterns of variation with respect to precipitation inputs (Fig. 2b and Fig. 2c). There were no obvious lags between rainfall and water level and discharge responses in the tanks, indicating similar synchronous responses to rainfall in these simple granular aquifers. However, there were clear magnitude differences in the water levels and volumes of discharge beneath the different land covers.

The air temperature, precipitation, water level and discharge data are also given in Table 2. There is little difference between the annual mean temperatures of the three hydrological years, which were 16.3 ℃, 16.8 ℃ and 16.0 ℃, respectively. In contrast, there were substantial differences in the annual amounts of rainfall, 978 mm, 1191 mm and 1443 mm respectively, which permit us to make some comparisons. The groundwater annual mean water level and discharge of the five model watersheds vary in the three hydrological years in response to the interannual differences of the rainfall. For water levels, the order was generally bare rock surface > bare soil surface > shrub land > cropped land > grassland; for discharge, it was always in the order - bare rock surface > bare soil surface > cropped land > shrub land > grassland (Fig. 2b, Fig. 2c and Table 2).

4.2. the stable isotopic compositions of the precipitation and groundwaters

The temporal variations in $\delta^{18}O$ and δD of the precipitation and groundwater in the five simulated watersheds, November 2015 to November 2018, are shown in Fig. 3. All of them can be viewed as sine curve functions. Stable isotopes in the precipitation were depleted in the rainy season and enriched in the dry season, which is consistent with findings from the Global Network of Isotopes in Precipitation (GNIP) (Rozanski et al., 1993) and the Chinese Network of Isotopes in Precipitation (CHNIP) (Liu et al., 2014). In contrast, the $\delta^{18}O$ and δD of the groundwaters (as measured at the springs) were enriched in the rainy season and depleted in the dry season, which indicates that the discharge of groundwater lags behind the precipitation. This observation is consistent with that of Comas-Bru and McDermott (2015), who observed such a "switch in seasonal patterns" in the top 60 cm of soil waters. In addition, we see that the five tanks exhibited similar behavior except for the bare rock, which had larger fluctuations and shorter phase lag times. The $\delta^{18}O$ and δD of all groundwaters under the five different land covers displayed obvious inter-annual variations over the three hydrological years. In contrast, the precipitation records display a strikingly uniform cyclicity.

The stable isotope statistics of the precipitation and groundwater during the three years are presented in Table 2. The $\delta^{18}O$ and δD of precipitation are represented by their annual amount-weighted values, which quantitatively determine the differing isotopic inputs to the aquifers. The annual amount-weighted values of precipitation during the three years were −8.3‰, −10.4‰ and −7.7‰ for $\delta^{18}O$, and −54.2‰, −72.0‰ and −49.5‰ for δD (Table 2). The arithmetic annual means of groundwater under different land covers over the three years were, in the bare rock tank $\delta^{18}O$ −9.1‰, −9.0‰ and −8.9‰, and δD −62.6‰, −60.8‰ and −60.2‰; bare soil tank $\delta^{18}O$ −9.0‰, −8.5‰ and −8.5‰, and δD −64.9‰, −62.6‰ and −62.5‰; cropped land tank $\delta^{18}O$ −9.1‰, −8.6‰ and −8.8‰, and δD −65.1‰, −62.7‰ and −64.4‰. In the grassland and shrub land, these annual means were −9.2‰, −8.9‰ and −8.9‰ for $\delta^{18}O$ and −63.1‰, −61.2‰ and −61.8‰ for δD, and −9.1‰, −8.4‰ and −8.6‰ for $\delta^{18}O$ and −65.0‰, −60.5‰ and −62.4‰ for δD, respectively (Table 2).

Student's t-test and F-tests with 0.05 confidence levels were conducted for $\delta^{18}O$ and δD in the precipitation and groundwaters over the three years. Student's t-test clearly differentiates the precipitation from all groundwaters for both isotopes. Groundwaters under the five simulated watersheds did not statistically differ from one another except for bare rock v bare soil, bare soil v grassland, and grassland v shrub land in the case of $\delta^{18}O$, bare rock v cropped land and bare soil v cropped land in the case of δD. F-tests also showed that precipitation differed significantly from groundwater, and that the groundwater passing

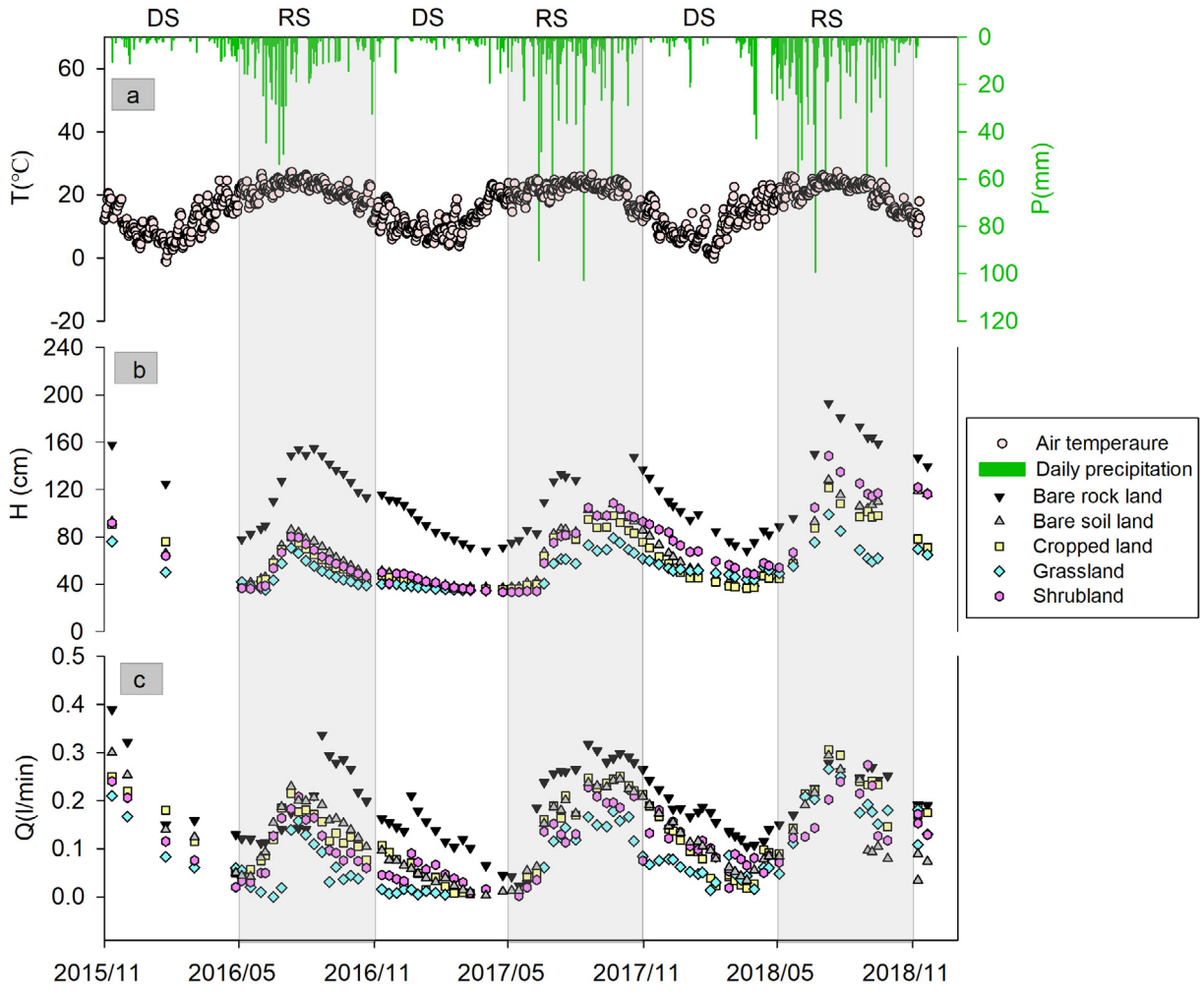

Fig. 2. Seasonal variations in main daily air temperature (T), daily precipitation (P) (a), water levels (H) (b) and discharges of groundwater (Q) (c) at the Shawan study site. "DS" and "RS" denote dry and rainy seasons, respectively.

through the bare rock tank was significantly different statistically from the other four types of groundwater in both $\delta^{18}O$ and δD. $\delta^{18}O$ also differed significantly in the bare soil v cropped land and cropped land v grassland pairs.

4.3. the fitted seasonality characteristics of precipitation and groundwater

In Fig. 3, we observe sinusoidal variations in $\delta^{18}O$ and δD in the precipitation and groundwater records between November 2015 and November 2018. The sine function form of the precipitation $\delta^{18}O$ and δD during the three years is displayed in Fig. 4. It is smooth, with little distortion and unremarkable annual differences caused by the big differences in the actual amounts of rain that fell in these successive wet seasons. However, from Fig. 3, there are obvious annual differences in groundwater $\delta^{18}O$ and δD, all of which except the bare rock showed little seasonal variation during the months between September 2016 and August 2017, an effective span of one hydrologic year. As a consequence of these behavior, if the groundwater isotopic data for the entire period were to be fitted with one single function, the accuracy of fit would be significantly reduced: thus, in Fig. 5 we fit the three climatic years of groundwater data separately, with 0.05 confidence level. The fitted results for precipitation and groundwater are presented in Table 3, which includes the fitted annual mean of $\delta^{18}O$ and δD, fitted sine amplitudes of $\delta^{18}O$ and δD (A), fitted periods of the cycle (b), the phase lags (c), statistical significance value (p) and correlation coefficient (R^2) to the sine curves.

From Table 3, all fitted sine curves are significant ($P < 0.05$), especially the two years, November 2015-October 2016 and November 2017-October 2018 ($P < 0.0001$). As noted, there was remarkably little seasonal variation in groundwater $\delta^{18}O$ and δD between September 2016 and August 2017; as a consequence, its correlation coefficients are relatively poor, 0.33 to 0.47 for $\delta^{18}O$, 0.34 to 0.42 for δD. The correlation coefficients in the other two years are strong, from 0.68 to 0.94 for $\delta^{18}O$, 0.79 to 0.93 for δD. This is higher than in the precipitation (0.59 for $\delta^{18}O$ and 0.64 for δD), because the precipitation values derive from individual rainstorms in this study. In addition,

Table 2
The annual mean data for air temperature, precipitation, water levels and discharge of groundwaters, and stable isotopic compositions of precipitation and groundwaters in the simulated watersheds, from November 2015 to October 2018.

Period	Water type	Air temperature (°C)	P (mm/a)	Water level(cm)		Discharge (L/min)		$\delta^{18}O$ (‰)			δD (‰)		
				Mean[a]	STDEV[b]	Mean[a]	STDEV[b]	Mean[a]	STDEV[b]	Range[c]	Mean[a]	STDEV[b]	Range[c]
2015/11–2016/10	Precipitation	16.3	978					−8.3	4.3	23.0	−54.2	37.5	187.5
	Bare rock			125.0	25.4	0.20	0.08	−9.1	1.1	3.2	−62.6	9.0	26.7
	Bare soil			62.7	15.7	0.15	0.07	−9.0	0.4	1.5	−64.9	2.9	10.3
	Cropped			58.3	14.7	0.13	0.06	−9.1	0.6	2.0	−65.1	4.3	12.2
	Grassland			49.2	11.8	0.07	0.06	−9.2	0.5	1.6	−63.1	3.9	11.6
	Shrubland			58.0	15.6	0.11	0.06	−9.1	0.5	1.7	−65.0	3.8	11.5
2016/11–2017/10	Precipitation	16.8	1191					−10.4	4.4	18.9	−72.0	38.9	161.7
	Bare rock			100.4	24.7	0.20	0.09	−9.0	1.0	3.6	−60.8	8.8	29.6
	Bare soil			64.5	26.2	0.12	0.09	−8.5	0.6	2.1	−62.6	4.3	16.1
	Cropped			58.8	23.2	0.11	0.10	−8.6	0.5	1.8	−62.7	3.6	14.3
	Grassland			48.7	16.5	0.06	0.06	−8.9	0.6	1.7	−61.2	4.3	12.4
	Shrubland			62.5	27.9	0.09	0.07	−8.4	0.4	1.3	−60.5	3.3	11.9
2017/11–2018/10	Precipitation	16.0	1443					−7.7	4.0	16.4	−49.5	34.5	133.4
	Bare rock			115.4	39.7	0.19	0.05	−8.9	1.7	5.1	−60.2	13.6	40.8
	Bare soil			71.0	30.2	0.16	0.07	−8.5	1.2	3.2	−62.5	10.3	28.2
	Cropped			63.8	26.9	0.16	0.08	−8.8	1.5	4.0	−64.4	12.0	31.8
	Grassland			57.9	13.4	0.12	0.07	−8.9	1.2	3.1	−61.8	9.8	24.9
	Shrubland			83.3	31.1	0.14	0.06	−8.6	1.2	3.0	−62.4	10.6	25.8
2015/11–2018/10	Precipitation	16.4	1204					−8.7	4.3	23.0	−58.1	37.2	187.5
	Bare rock			113.1	32.1	0.20	0.08	−9.0	1.3	5.1	−61.4	10.3	40.8
	Bare soil			66.8	25.2	0.14	0.08	−8.7	0.8	3.4	−63.5	6.2	29.2
	Cropped			60.4	22.5	0.13	0.08	−8.9	0.9	4.0	−64.1	7.2	31.8
	Grassland			52.0	14.8	0.08	0.07	−9.0	0.8	3.2	−62.3	6.3	24.9
	Shrubland			68.6	28.2	0.11	0.07	−8.8	0.8	3.1	−62.8	6.6	25.8

[a] The mean $\delta^{18}O$ and δD of precipitation are expressed by the annual amount-weighted values of $\delta^{18}O$ and δD, and other means are based on arithmetic averages.
[b] STDEV the standard deviation.
[c] The difference between the maximum value and the minimum value.

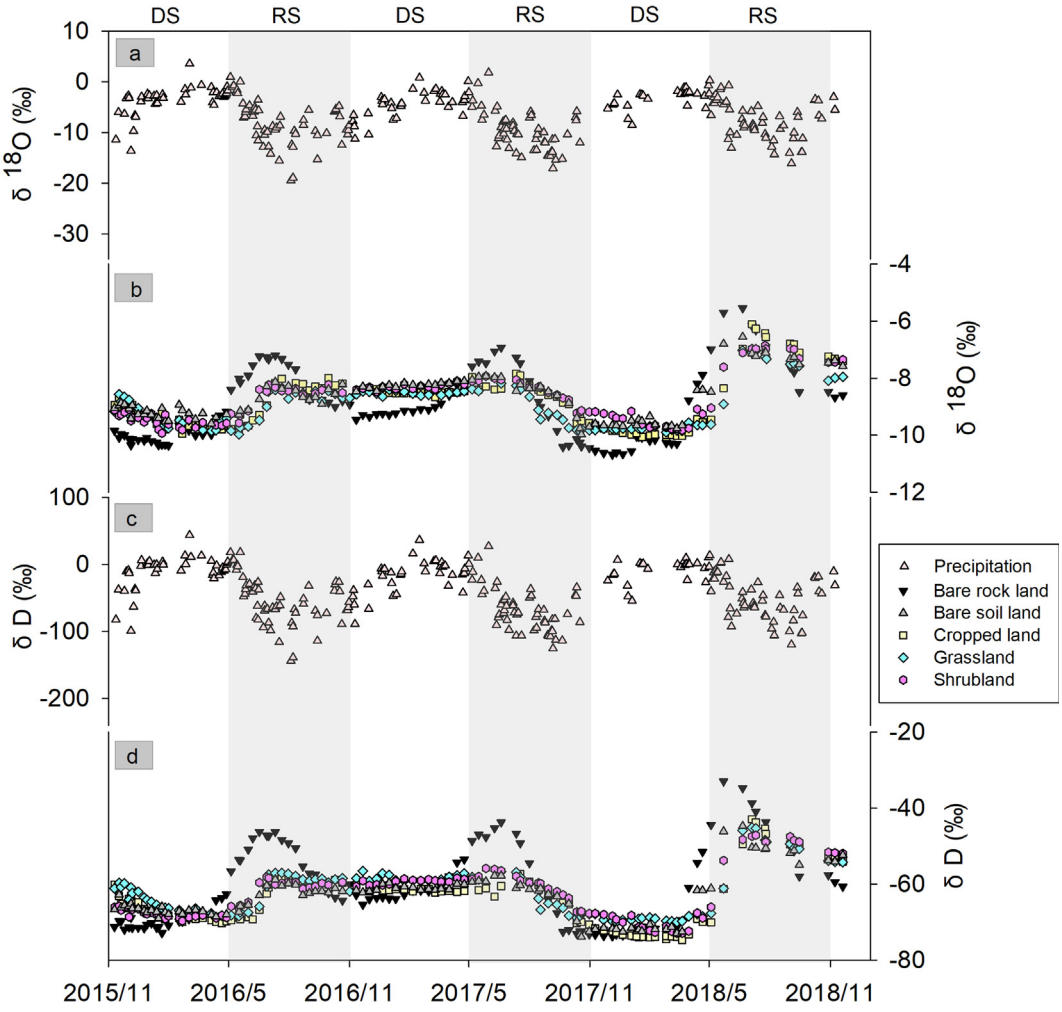

Fig. 3. Seasonal variations in $\delta^{18}O$ and δD of the precipitation and groundwater in the five simulated watersheds. (a) and (b) are $\delta^{18}O$ of the precipitation and groundwater respectively. (c) and (d) are δD of the precipitation and groundwater respectively. "DS" and "RS" denote dry season and rainy season, respectively.

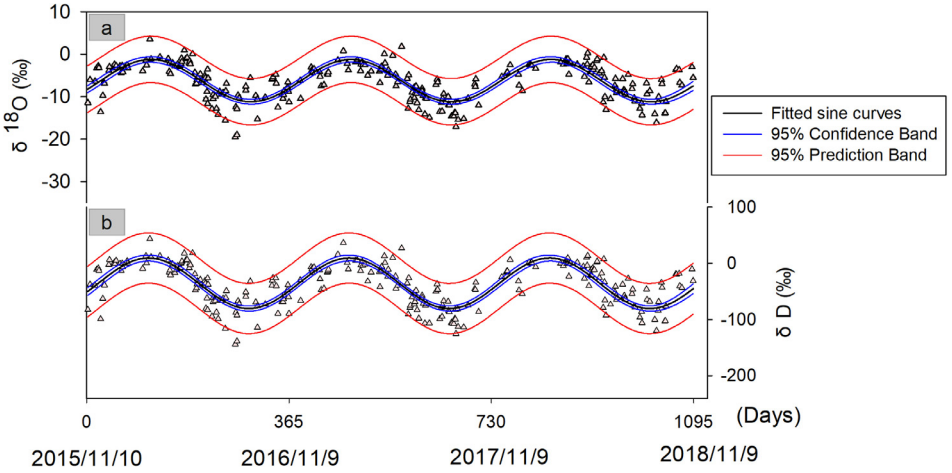

Fig. 4. The best-fit sine curves (with 0.05 confidence level) of $\delta^{18}O$ and δD in the precipitation for the full period between November 2015 and November 2018. (a) and (b) are $\delta^{18}O$ and δD in precipitation respectively. Detailed fitted results are summarized in Table 3.

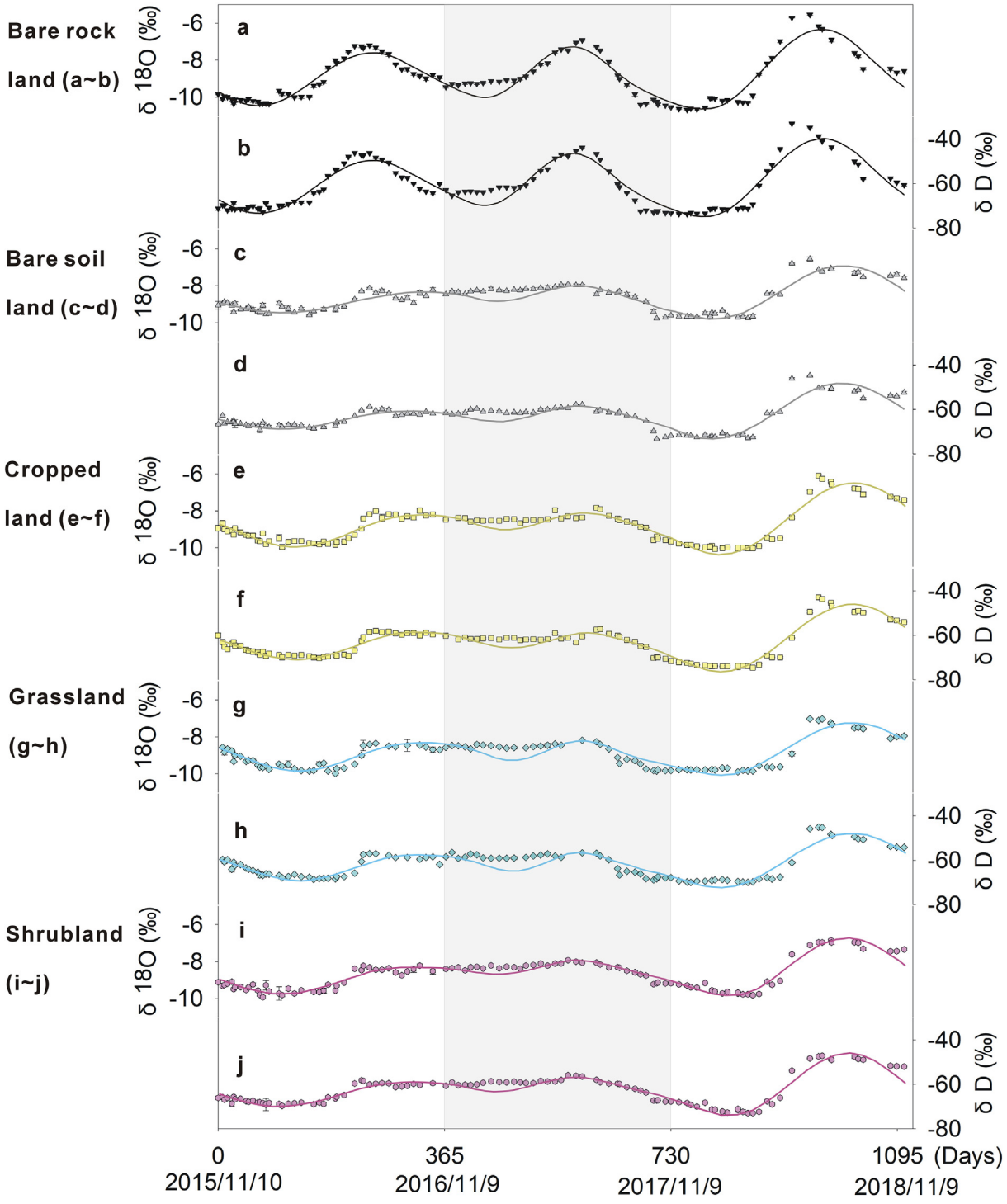

Fig. 5. The best-fit sine curves (with 0.05 confidence levels) of $\delta^{18}O$ and δD in groundwater under the different land covers, November 2015 - October 2018. Detailed fitted results are summarized in Table 3.

note that the fitted periods of cycle b for the second fitted year, from 225 days to 283 days for $\delta^{18}O$ and from 222 days to 282 days for δD, were substantially shorter than 365 days, i.e. a typical sinusoidal cycle. The amplitude ratios (A/A_0) of groundwaters to the precipitation were calculated from the fitted sine amplitudes (Table 3). Based on the periods of the cycles and the phase lags of the fitted results, the lag times of groundwater discharge behind the precipitation input under the different land covers were estimated with Eq. (5) and are also given in Table 3.

Table 3
Summary of results of fitting sine functions to seasonal variations in $\delta^{18}O$ and δD in the precipitation and groundwaters (with 0.05 confidence level), and the amplitude ratios (A/A_0) and the calculated phase lag times between groundwater and precipitation ($\triangle t$) were also given.

Period	Water type	$\delta^{18}O$ fitted results								δD fitted results							
		I (‰)	A ± SE	b (days)	c ± SE (rad)	R^2	p	A/A_0[a] ± SE (%)	$\triangle t$[b] ± SE (Days)	I (‰)	A ± SE	b (days)	c ± SE (rad)	R^2	p	A/A_0[a] ± SE (%)	$\triangle t$[b] ± SE (Days)
2015/11–2016/10	Bare rock	−9.0	1.43 ± 0.07	369	3.62 ± 0.09	0.92	≤0.0001	28.6 ± 1.5	133 ± 9	−61.4	11.68 ± 0.59	367	3.66 ± 0.10	0.91	≤0.0001	26.0 ± 1.2	134 ± 10
	Bare soil	−8.9	0.48 ± 0.05	380	3.00 ± 0.18	0.68	≤0.0001	9.6 ± 0.5	178 ± 22	−64.6	3.64 ± 0.32	380	3.03 ± 0.14	0.79	≤0.0001	8.1 ± 0.4	180 ± 17
	Cropped	−9.0	0.85 ± 0.05	380	2.68 ± 0.10	0.86	≤0.0001	17.1 ± 0.9	197 ± 15	−64.6	6.02 ± 0.37	380	2.67 ± 0.10	0.87	≤0.0001	13.4 ± 0.6	202 ± 15
	Grassland	−9.1	0.73 ± 0.06	359	2.45 ± 0.11	0.82	≤0.0001	14.6 ± 0.7	193 ± 14	−63.2	5.56 ± 0.41	349	2.39 ± 0.11	0.83	≤0.0001	12.4 ± 0.6	193 ± 13
	Shrubland	−9.1	0.70 ± 0.05	380	3.02 ± 0.12	0.83	≤0.0001	14.1 ± 0.7	176 ± 15	−64.4	5.12 ± 0.33	380	3.10 ± 0.11	0.87	≤0.0001	11.4 ± 0.5	176 ± 13
2016/11–2017/10	Bare rock	−8.6	1.36 ± 0.11	283	3.34 ± 0.16	0.83	≤0.0001	27.3 ± 1.4	88 ± 11	−57.9	11.63 ± 0.88	282	3.34 ± 0.15	0.85	≤0.0001	25.9 ± 1.2	91 ± 11
	Bare soil	−8.3	0.41 ± 0.10	260	2.88 ± 0.45	0.33	0.0080	8.3 ± 0.5	90 ± 28	−61.2	3.38 ± 0.86	264	2.81 ± 0.43	0.34	0.0059	7.5 ± 0.4	101 ± 27
	Cropped	−8.5	0.45 ± 0.09	253	2.35 ± 0.35	0.47	0.0002	9.0 ± 0.5	106 ± 22	−62.2	3.33 ± 0.75	250	2.11 ± 0.42	0.40	0.0013	7.4 ± 0.4	117 ± 26
	Grassland	−8.8	0.52 ± 0.12	225	−4.51 ± 0.45	0.40	0.0021	10.4 ± 0.6	102 ± 23	−60.5	4.07 ± 0.95	222	−4.52 ± 0.44	0.41	0.0019	9.1 ± 0.5	104 ± 22
	Shrubland	−8.3	0.36 ± 0.07	250	2.58 ± 0.31	0.47	0.0002	7.3 ± 0.4	94 ± 19	−59.9	3.10 ± 0.66	250	2.55 ± 0.36	0.42	0.0007	6.9 ± 0.3	100 ± 22
2017/11–2018/10	Bare rock	−8.5	2.17 ± 0.17	380	3.84 ± 0.18	0.87	≤0.0001	43.5 ± 2.3	127 ± 16	−57.2	17.56 ± 1.29	380	3.85 ± 0.17	0.88	≤0.0001	39.1 ± 1.9	131 ± 16
	Bare soil	−8.3	1.44 ± 0.10	420	3.72 ± 0.17	0.89	≤0.0001	28.5 ± 1.5	169 ± 23	−60.6	12.59 ± 0.93	420	3.74 ± 0.17	0.88	≤0.0001	28.0 ± 1.3	164 ± 17
	Cropped	−8.4	1.92 ± 0.10	429	3.56 ± 0.11	0.94	≤0.0001	38.5 ± 2.0	178 ± 14	−61.2	15.22 ± 0.79	426	3.55 ± 0.11	0.93	≤0.0001	33.9 ± 1.6	180 ± 13
	Grassland	−8.7	1.41 ± 0.10	429	3.59 ± 0.15	0.89	≤0.0001	28.3 ± 1.5	176 ± 18	−59.8	12.17 ± 0.84	425	3.56 ± 0.14	0.90	≤0.0001	27.1 ± 1.3	179 ± 17
	Shrubland	−8.3	1.56 ± 0.10	380	3.17 ± 0.11	0.91	≤0.0001	31.3 ± 1.6	168 ± 12	−59.8	13.91 ± 0.84	380	3.17 ± 0.11	0.91	≤0.0001	30.9 ± 1.5	172 ± 12
2015/11–2018/10	Precipitation	−6.2	4.98 ± 0.25	361	5.84 ± 0.08	0.59	≤0.0001			−35.5	44.96 ± 2.08	362	5.92 ± 0.07	0.64	≤0.0001		

Note: Seasonal variations in $\delta^{18}O$ and δD follow the sine function form below:

$$\delta = I + A\sin[(2\pi t/b) + c] \quad (1)$$

where δ is the isotopic composition, I is the sine offset on the δ axis, A is the seasonal amplitude of the sine function, b is the period of the sinusoidal cycle, t is time in days, and c is the phase lag in radians.

[a] The amplitude ratios of groundwater to precipitation.

[b] The phase lag times between groundwater and precipitation under the different land covers, calculated by Eq. (5). "SE" denotes standard error. "R^2" and "p" denote correlation coefficient and statistical significance value respectively.

5. DISCUSSION

5.1. Stable isotopes in precipitation determined by monsoon activities

The stable oxygen and hydrogen isotopic composition of precipitation are controlled by various factors, including vapor sources, temperature, rain-out effects, etc. Previous studies have shown a strong correlation between rainfall isotopic values and temperature at the global scale (Dansgaard, 1964; Yurtsever and Gat, 1981, etc), but such correlation does not appear in every region. For example, there is no clear correlation between rainfall isotopic values and the temperatures in the tropics and mid-latitudes of the Northern Hemisphere, but some inverse correlation with the quantities of rainfall (Lawrence et al., 1982; White and Gedzelman, 1984). Given that the Puding experimental site in southwest China lies just within that area, in Fig. 6 we show the quantitative relationships between rainfall and $\delta^{18}O$ and δD, at the individual event scale (Fig. 6a, b) and at the monthly scale by aggregating the event data (Fig. 6c, d). There are negative linear correlations between $\delta^{18}O$, δD and the amounts of rainfall at both timescales but, although these relationships are statistically significant ($p < 0.0001$), their R^2 correlation coefficients are low (from 0.14 to 0.33), indicating that factors other than simply rainfall amounts are at play.

In southwest China, the stable isotope composition of precipitation is chiefly controlled by conditions in the winter monsoon and summer monsoon, with heavier and lighter isotopic compositions respectively (Zhang et al., 2007; Chen and Li, 2018; Zhao et al., 2018). As shown in Fig. 2a and Fig. 7, and consistent with other studies from nearby regions, $\delta^{18}O$, d-excess, temperature and precipitation in our study all exhibit annual cycles, with relatively low $\delta^{18}O$ and d-excess values but high temperature, amount and frequency of precipitation during the rainy season. In detail, from early April to July, as the summer monsoon

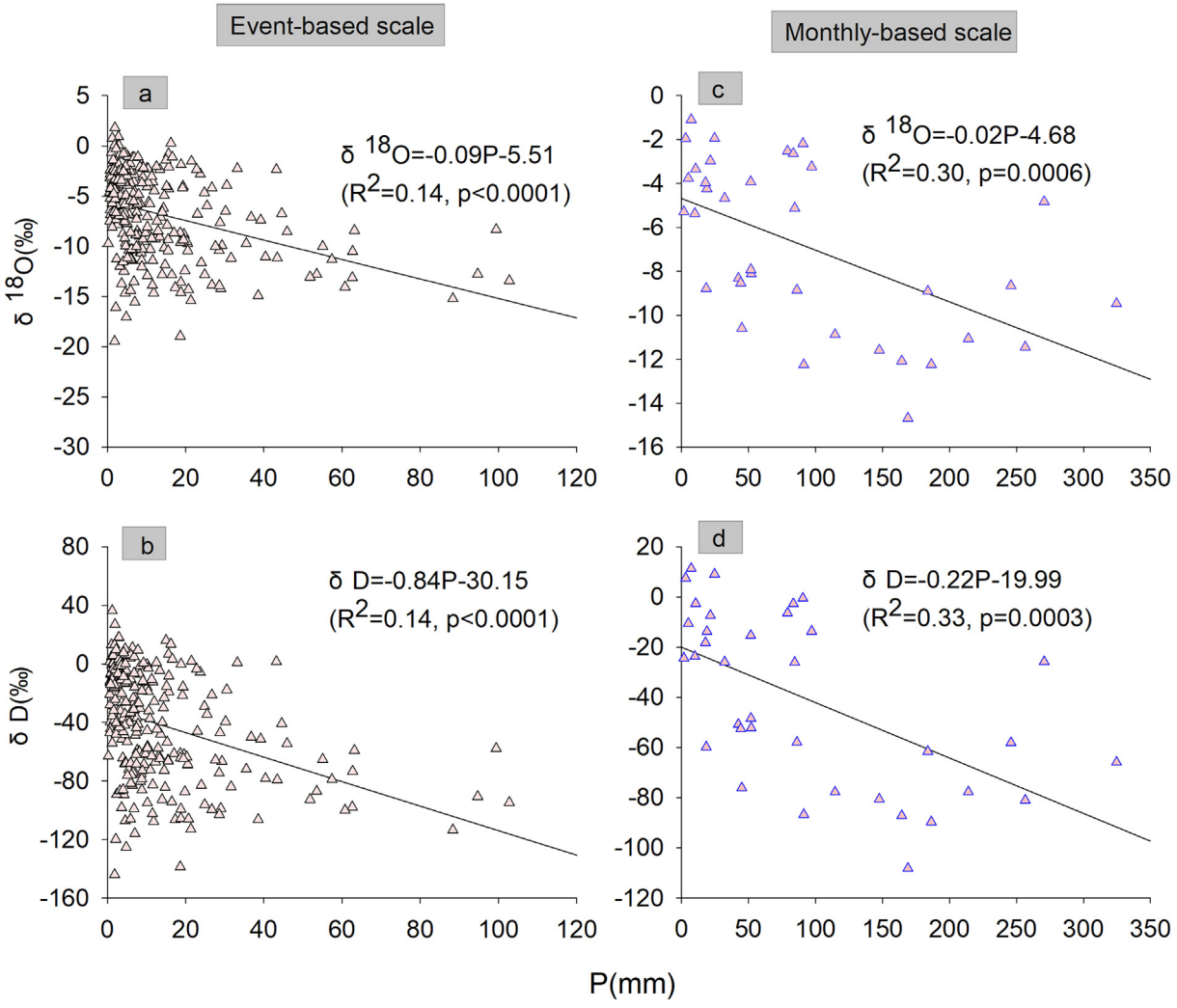

Fig. 6. The correlations (0.05 confidence level) between $\delta^{18}O$ and δD in the precipitation and the amounts of precipitation, at different timescales: (a) and (b) are $\delta^{18}O$ and δD respectively v rainfall amounts at the event-based scale. (c) and (d) are $\delta^{18}O$ and δD respectively v rainfall amounts aggregated to the monthly scale.

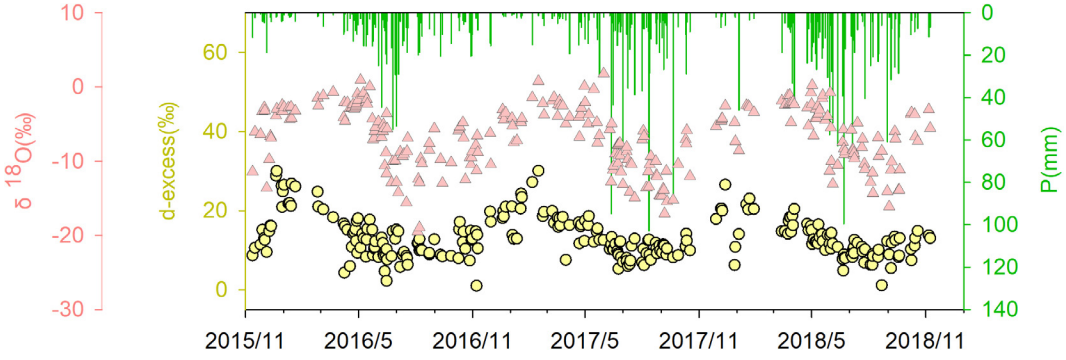

Fig. 7. The temporal variations in daily rainfall amount, d-excess and $\delta^{18}O$ of precipitation at the study site.

becomes established, there are decreases of $\delta^{18}O$ and d-excess, indicating that the percentage of water vapor from oceanic sources is gradually increasing until it dominates: d-excess can be an important indicator of moisture sources. From July to late October, low and relatively consistent d-excess values indicate dominance by oceanic vapor sources that result in lower, although fluctuating, $\delta^{18}O$ values even as the amount of rainfall during this period typically decreases. From November, when the summer monsoon retreats, $\delta^{18}O$ and d-excess both increase as the amount and frequency of precipitation fall to the annual minima. Such varying monsoon- related changes of vapor sources create and pace the cycles of $\delta^{18}O$, d-excess, and precipitation, and thus explain the poor correlation between $\delta^{18}O$ and rainfall amounts at different timescales, as presented here and in previous studies in this transitional region (Zhang et al., 2007).

5.2. Temporal variation of groundwater stable isotope values in the simulated watersheds

5.2.1. Amplitude of groundwater $\delta^{18}O$ and δD cycles determined by the land covers

From the fitted sine curve amplitudes of the precipitation and the groundwaters given in Table 3, the amplitudes in groundwaters in the bare rock tank were reduced to 27% ~ 44% for $\delta^{18}O$ and 26% ~ 39% for δD of the ranges measured in the original meteoric precipitation. The amplitudes in the other four tanks were reduced to 7% ~ 39% ($\delta^{18}O$) and 7% ~ 34% (δD) of the original over the full period of investigation, i.e. the amount of damping of the $\delta^{18}O$ signal ranged from 56~73% and of δD from 61~74 in the bare rock tank, and from 61~93 ($\delta^{18}O$) and 66~93 (δD) in other four tanks. The inter-year differences of amplitude ratios that existed in all of the groundwaters over the three fitted years will be discussed in Section 5.3. In sum, the seasonal variations of $\delta^{18}O$ and δD in the precipitation were substantially damped in all recharged groundwaters. The amplitude ratios (damping effects, i.e. 1- amplitude ratio) of $\delta^{18}O$ and δD in the four soil and vegetated tanks are close to each other, but are statistically significantly different from those of the bare rock tank, a finding that is supported by the conclusions of the F-tests.

It is significant to note that the amplitude ratios of $\delta^{18}O$ and δD in the bare rock land differ from those in the four soil-topped lands that are closely similar to each other. Why do the $\delta^{18}O$ and δD amplitude ratios display such differences? As mentioned above, when precipitation recharges groundwater through the complex sequence of vegetation-litter-soil–bedrock aquifer, it will mix with any pre-existing water along the seepage paths, which reduces the seasonal variations of oxygen and hydrogen isotope ratios. The degree of damping is determined chiefly by evaporation, the hydrodynamic conditions such as velocity of flow and the isotopic composition of the pre-existing water (Eichinger et al., 1984; Clark and Fritz, 1997; Bradley et al., 2010; Luo et al., 2014).

In our study, all simulated watersheds are of the same size and have identical boundary conditions, which implies that their groundwater discharges may be used as an important indicators of their hydrodynamic vigor. From the data in Fig. 2c and Table 2, the three-year mean annual discharges were 0.20 L/min in the bare rock tank, 0.14 L/min for bare soil tank, 0.13 L/min for cropped land, 0.11 L/min for shrub land and 0.08 L/min for grassland, placing the vigor of their groundwater circulation in that order. Based on a previous study of the Shawan Karst Test Site (Hu et al. 2018), these five watersheds suffered evaporation losses (the ratio of evaporation to precipitation) in the order: bare soil > cropped land > shrub land > grassland > bare rock, the mean annual evaporation losses being 36.2% for bare soil, 17.7% for cropped land, 16.6% for shrub land, 9.0% for grassland and only 5.9% for bare rock. The synchronous behavior of $\delta^{18}O$ and δD in the groundwaters indicate that there is negligible influence by any water–rock isotopic interactions in these tank experiments (Fig. 5 and Table 3).

Given the identical isotopic inputs of precipitation and negligible influence of water–rock interactions on groundwaters in our study, the damping of $\delta^{18}O$ and δD under different land covers is mainly determined by the vigor of the hydrodynamic conditions (chiefly, rate of infiltration) and evaporation. The notably lower damping seen in the bare rock tank is due to most rapid infiltration that results in lowest evaporation losses, attributable to the absence of soil and plants to intercept the rain and impede flow beneath it. The damping effects among the four soil-covered surfaces are not significantly different from each other statistically, which can be attributed to a co-dominance of hydrodynamic conditions and evaporation. For example, the

amount of damping in the bare soil, where no vegetation cover results in both highest discharge and greatest evaporation loss in the four lands, is similar to that of grassland where the densest vegetation cover results in the smallest discharge but least evaporation. As a consequence it is seen that these vegetation covers had limited influence in differentiating the damping of the seasonal isotopic variations. In sum, while the differing vegetation covers created interesting variations, the presence of the uniform 0.5 m soil cover in these model tanks had the most significant effect on the dampening of O and H isotopic seasonal variations recorded in the rainfall.

5.2.2. Phase lag times under the different land covers

The phase lag times ($\triangle$t) between groundwater and precipitation in the five simulated watersheds (calculated with Eq. (5)) are summarized in Table 3. It is seen that the phase lags of the $\delta^{18}O$ and δD pairs in each individual experiment throughout the period of record are very close to each other, being statistically indistinguishable in fact. The phase lag times under any given land cover in different years are also statistically indistinguishable, with the notable exception of the middle hydrologic year, November 2016 - October 2017. The anomalies there are due to the limited seasonal variation resulting in some distortion of the fitted sine functions in that year; as noted above, their cycle b fitted periods were substantially shorter than 365 days and, as a consequence, their calculated phase lag times are set aside here as being unrepresentative. The other two fitted years exhibited the high degree of stability in groundwater flow behavior that might be expected in such simple model aquifers. Based on their data, the average lags and standard errors were 131 ± 13 days in the bare rock tank, 171 ± 20 days in bare soil, 189 ± 14 days in the cropped land, 185 ± 16 days in grassland and 173 ± 13 days in the shrub land.

The phase lag times of groundwater being controlled chiefly by the hydrodynamic conditions in a watershed, given the identical sizes and basic hydrogeological conditions in the tanks, it is supposed that the phase lags will be broadly correlated with the individual groundwater discharges. The discharges of the five watersheds are: bare rock > bare soil > cropped land > shrub land > grassland (Fig. 2c and Table 2). The bare rock tank consistently has the largest discharge and shortest lag times. Although there are differences in discharge between the four soil-mantled surfaces, their difference in their lag times are not statistically significant from each other. Such differences may actually exist but be concealed by the error margins in the time calculations of the phase shifts: generalizing, however, the uniform 0.5 m soil cover was the predominant control on the phase lag times in these four different groundwaters.

The amplitude ratios of the five lands display stronger statistical differences than those of the phase lag times (Table 3). Many studies estimate groundwater lag times from the amplitude ratios by assuming that there are not significant evaporative effects. In our previous study, we also derived the groundwater lag times from the amplitude ratios, the calculated results being 190 days for bare rock, 509 days in the bare soil, 261 days in the cropped land, 381 days in grassland, 349 days in shrubland (Hu et al., 2018). Due to the influences of evaporation, all lag times estimated by amplitude ratios are higher than the lag times calculated through phase lag in this paper, even the bare rock with its limited evaporative losses. Comparing these two methods of estimating lag times in groundwaters, although the former shows better statistical precision, it is more susceptible to evaporation distorting the calculations. In addition, the inter-annual differences of the groundwater amplitude ratios under any given land cover (Table 3) during these successive hydrological years - caused by the inter-annual differences of amount-weighted $\delta^{18}O$ and δD in precipitation but not reflected in the temporal variations of $\delta^{18}O$ and δD in the rains - reminds us that the input of amount-weighted $\delta^{18}O$ and δD also needs to be carefully considered when applying the amplitude ratio method.

5.3. Responses of groundwater isotopic ratios to precipitation

Following the practice of Beddows et al. (2016), in Fig. 8c and 9c we have shifted the $\delta^{18}O$ and δD groundwater discharge records back in time by subtracting the phase lag periods under the different land covers. The years from November 2015 to November 2018 are divided into three dry and three rainy seasons. It is seen that the seasonal trends of comparative enrichment or depletion of $\delta^{18}O$ and δD in the groundwaters closely match those in the precipitation (Fig. 8a and Fig. 9a), with the exception of the 2016 rainy season that was noted above. Oxygen and hydrogen are isotopically depleted in the rainy seasons, enriched in the dry seasons.

$\delta^{18}O$ and δD groundwater enrichments and depletions also show some obvious inter-annual variations that are not so apparent in the precipitation records. The $\delta^{18}O$ and δD in all groundwaters were most depleted in Rainy Season 2 and most enriched in Dry Season 3 (Fig. 8c and Fig. 9c). According to the seasonal distribution of rainfall in the different years, summarized in Fig. 8a and Fig. 9a, we observe that the degree of isotopic depletion in the rainy seasons is not simply determined by their volumes of rainfall, e.g. there was similar depletion in the bare rock tank in Rainy Season 1 and Rainy Season 3, but their rainfalls were 789 mm and 1180 mm respectively. Given that isotopic compositions are impacted by evaporation, the δD-$\delta^{18}O$ plots were used to assess the influence of this process during the different seasons. In Fig. 10 it is seen that the groundwaters under the five covers deviate from the Local Meteoric Water Line (LMWL) to differing extents, indicating different degrees of evaporation: however, all of these groundwaters are displaying the same three isotopic responses to the three slightly differing rainy seasons. The δD-$\delta^{18}O$ plots indicate that the inter-annual differences in rainy seasons were determined by the isotopic input of the precipitation rather than reactions in the tanks and their different covers. Based on that, the amount and isotopic compositions of the individual rainfall events that were sampled (more than 5 mm in the dry season and more than 10 mm in the rainy season) are shown in Fig. 8a and Fig. 9a, and the amount-weighted $\delta^{18}O$ and δD of precipitation in Fig. 8b and Fig. 9b. The most depleted precipitation in Rainy Season

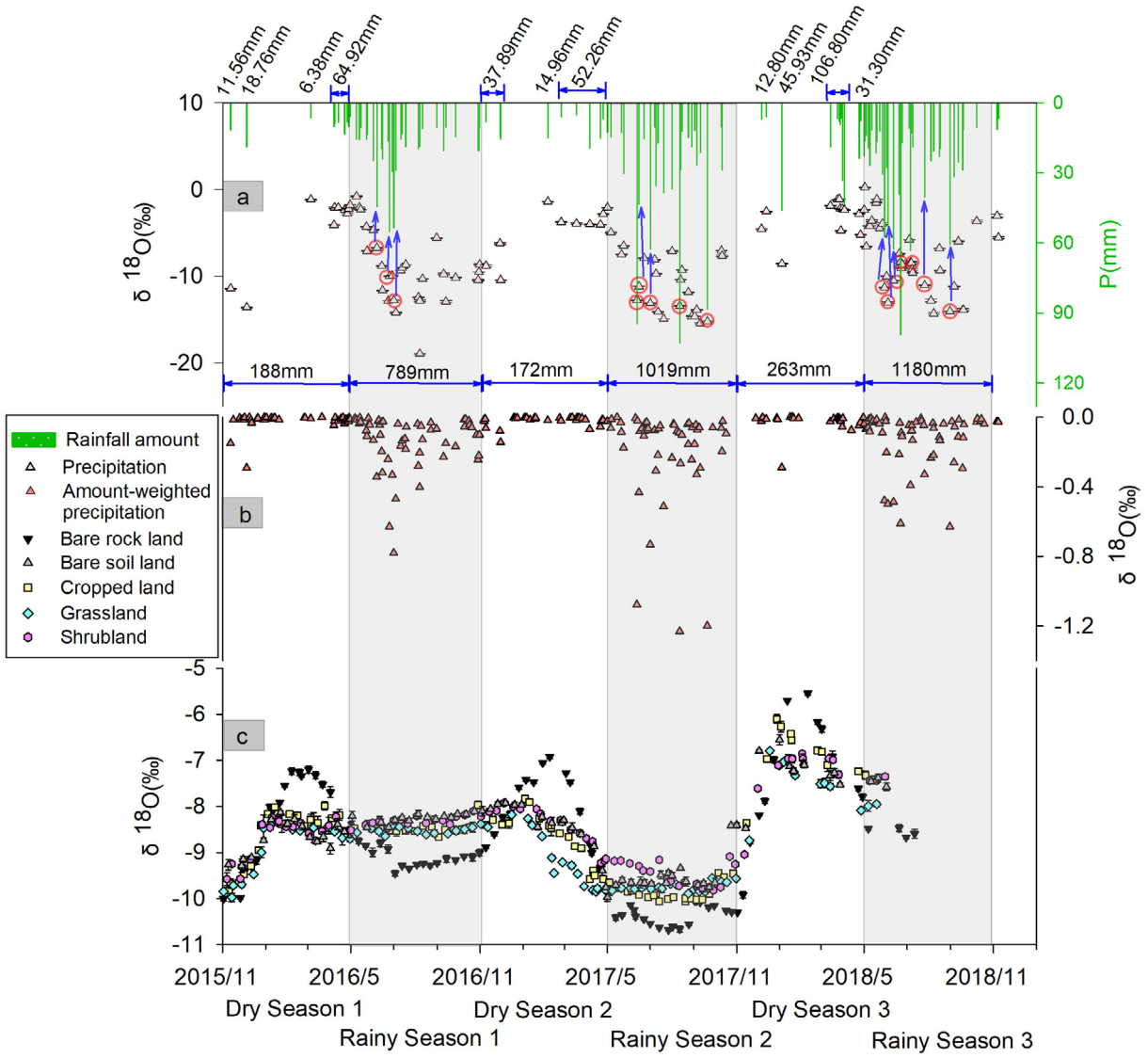

Fig. 8. The variations in individual rainfall amount, $\delta^{18}O$ of precipitation and groundwater from November 2015 to November 2018 including three dry seasons and three rainy seasons. (a) Individual rainfall amount and corresponding $\delta^{18}O$ of precipitation, including only the data for more than 5 mm in the dry season and more than 10 mm in the rainy season. The totals include all rainfall within the given season. (b) Amount-weighted $\delta^{18}O$ in the precipitation. (c) $\delta^{18}O$ of the groundwaters after subtracting the phase lag times between groundwater and precipitation.

2 came from relatively abundant heavy rains that depleted $\delta^{18}O$ and δD during that season. In contrast, although there were many heavy rains in Rainy Season 3 as well, their $\delta^{18}O$ and δD were not as depleted as in Rainy Season 2. As a result, the greater the amounts of depleted $\delta^{18}O$ and δD in the rainy seasons in the precipitation, the more depleted the $\delta^{18}O$ and δD in the groundwater will be. Accordingly, the anomaly of little seasonal variation of groundwater $\delta^{18}O$ and δD in Rainy Season 1 (2016) was caused by unusually small quantities of the highly depleted rainfall. Similarly, the inter-annual differences in groundwaters during the dry seasons were also dominated by the isotopic input from the precipitation, e.g. the isotopically enriched groupings seen in the discharge of all tanks in Dry Season 3 in Fig. 10 were caused by more rainfall that was isotopically enrichment (263 mm) than in the other two dry seasons.

The seasonal and inter-annual variations of $\delta^{18}O$ and δD occurring in precipitation can be conserved in groundwater under different land covers. It is interesting to note how the conserved signal strengths can vary with the land cover. As mentioned in Section 5.2.1, strongest conservation was in the bare rock tank, followed by lesser (and closely similar) amounts of conservation in the four soil-covered tanks. In addition, there were significant inter-annual variations in the amount-weighted $\delta^{18}O$ and δD in the precipitation, such that the seasonal input signal was readily smoothed by the soil when input strength was limited. This resulted in the groundwaters in the covered tanks failing to record strong seasonal signals during Rainy

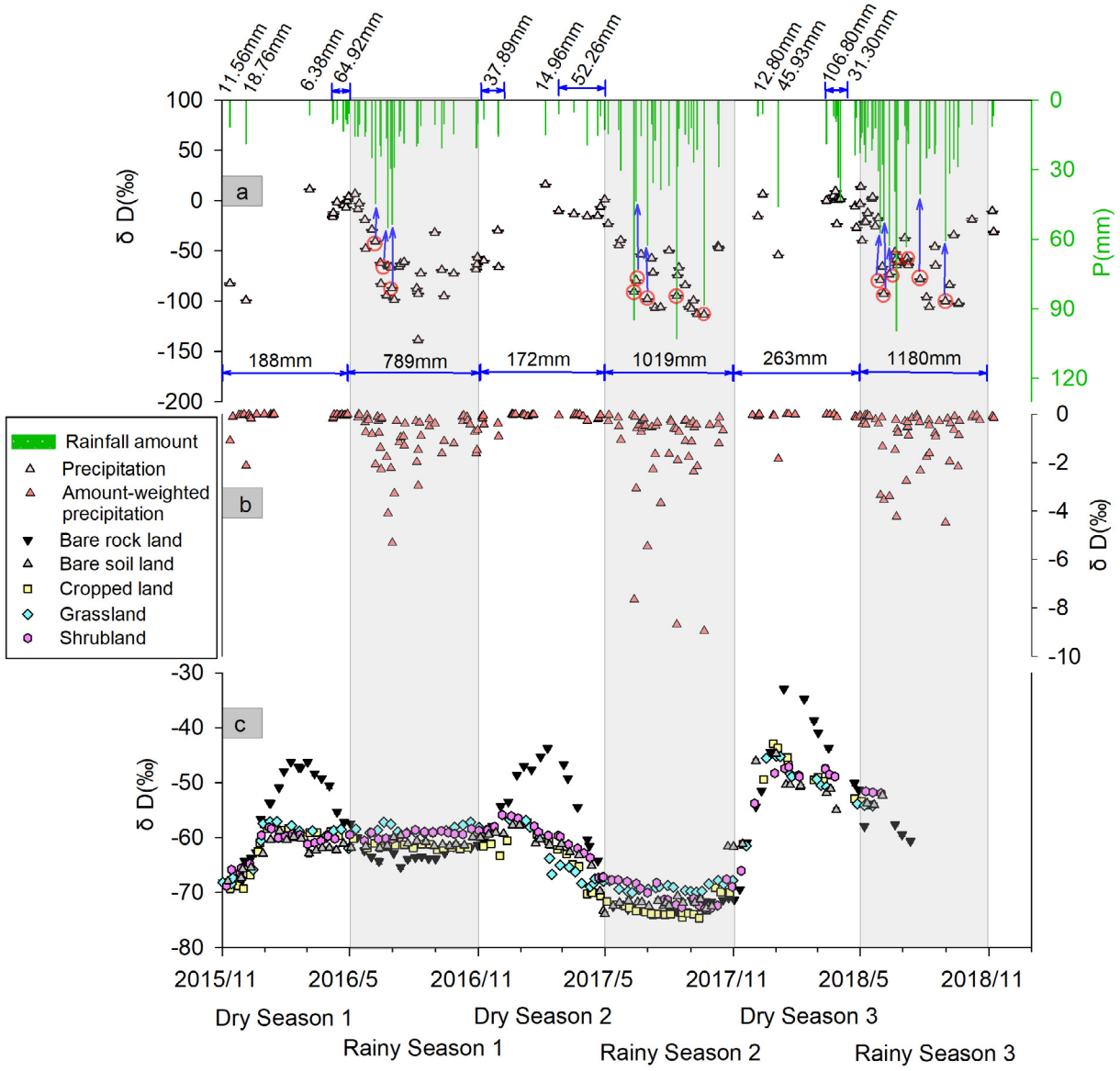

Fig. 9. The variations in individual rainfall amount, δD of precipitation and groundwater from November 2015 to November 2018 including three dry seasons and three rainy seasons. (a) Individual rainfall amount and corresponding δD of precipitation, including only the data for more than 5 mm in the dry season and more than 10 mm in the rainy season. (b) Amount-weighted δD in the precipitation. (c) δD of the groundwaters after subtracting the phase lag times between groundwater and precipitation.

Season 1 (Figs. 8, 9); such a loss of information would be difficult to detect in many speleothems, also. This confirms that, in the field, groundwaters under bare rock (such as rocky desertification terrains in temperate and tropical regions, karren fields and felsenmeer in arctic and alpine terrains) are better able to preserve seasonal $\delta^{18}O$ and δD signals in precipitation than terrains that have significant covers of residual or transported soils. These findings may have important implications for guiding the choice of carbonate samples for well-preserved isotopic seasonality inherited from precipitation, e.g. drip water or stalagmite samples in caves for better high-resolution paleoclimate research in the future.

5.4. Comparisons with groundwaters precipitating calcite speleothems in natural caves.

The purpose of this contribution is to provide a baseline set of data for comparative studies of the conservation of seasonal and inter-annual variations of $\delta^{18}O$ and δD in groundwaters flowing through carbonate aquifers. The Shawan model aquifers are contained in identical limestone gravels and possess uniform primary porosities. Only their soil and plant covers are varied. Previous studies have reported on their water chemical behavior over one or more hydrological years (Zeng et al., 2017), using the stable isotope data (δD excess) to estimate evaporation and

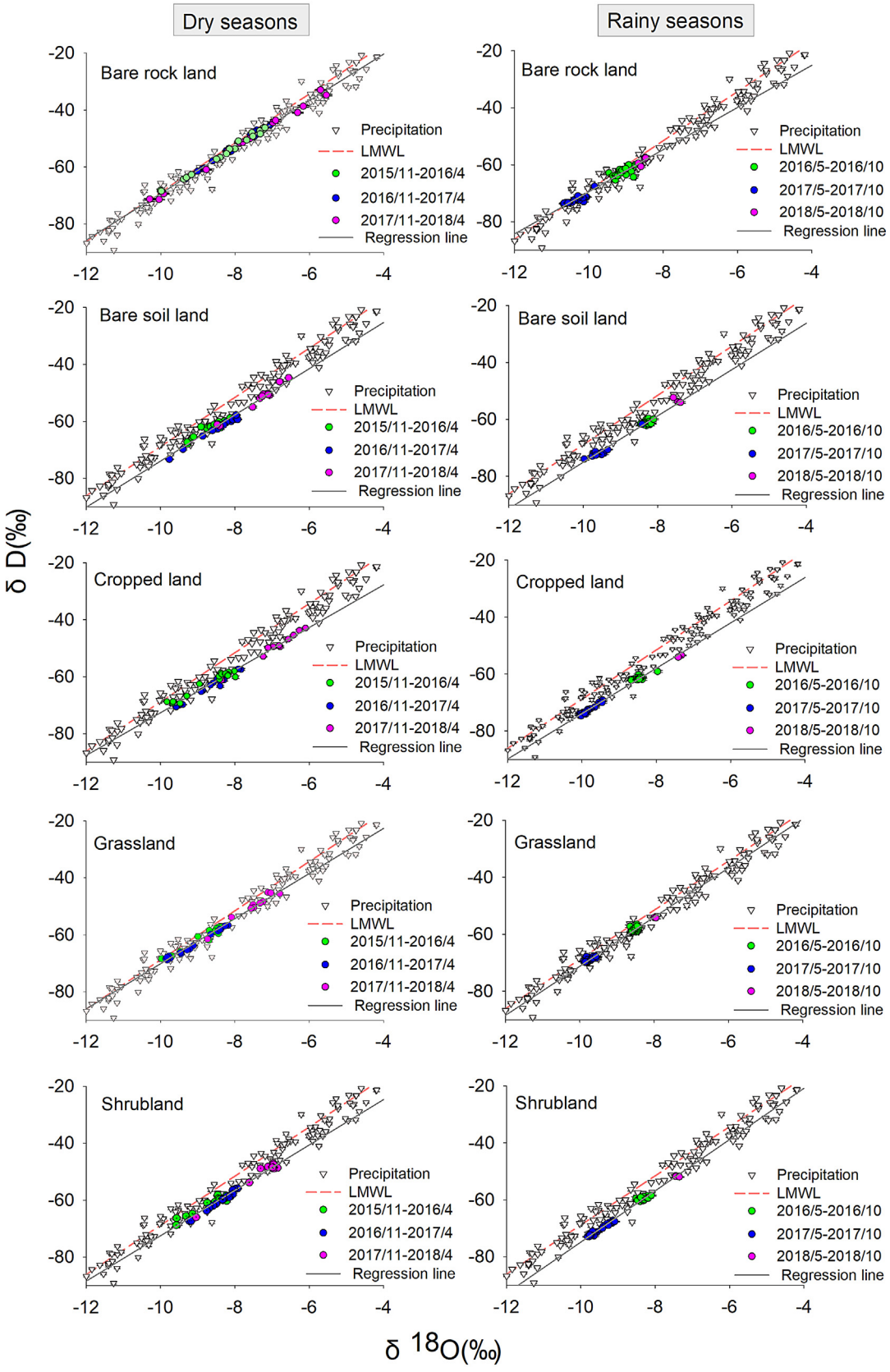

Fig. 10. The δD-δ^{18}O plots of the precipitation and all tank groundwaters (after subtracting their phase lag times) under dry and rainy seasons. (Left) δD-δ^{18}O plots under different land covers for the three dry seasons between November 2015 and November 2018. (Right) δD-δ^{18}O plots under different land covers for the three rainy seasons between November 2015 and November 2018. The Local Meteoric Water Line (LMWL) with a 0.05 confidence level from the precipitation data is plotted as a pink dashed line. For comparison the regression line for the groundwater data (0.05 confidence level) is shown as a gray solid line.

transpiration losses (Hu et al., 2018). It has also been shown that their artificial spring waters are aggressive (undersaturated) or supersaturated wrt to calcite and dolomite, at different times; i.e. despite the small dimensions of the model tanks, the groundwaters would be capable of precipitating calcite speleothems when the necessary physical and chemical conditions arise (Zeng et al., 2017).

It is interesting to compare these experimental tank results to equivalent field results for drip waters that are, in net terms, precipitating calcites in natural caves. There are many such studies in the modern literature but few of them have investigated the proportional conservation of seasonal, etc. $\delta^{18}O$ and δD signals in the source precipitation. As mentioned above, many speleothem drip waters typically show little or no seasonal isotopic variations despite $\delta^{18}O$ in the meteoric precipitation ranging > 15‰. For example, seasonal variations of $\delta^{18}O$ in most published studies have been found to be < 4‰, e.g. 1.2‰ in Luo et al. (2014), 2.9‰ in Chen and Li (2018), 3.5‰ in Wu et al. (2014) from sites in China, 2.2‰ in Beddows et al. (2016) on the Pacific coast of Canada, totally smoothed in the Yonge et al. (1985) transect of the USA noted above, in Genty et al. (2014) in southern France, Duan et al. (2016) in southern China, etc., compared to 1.3‰ ~ 5.1‰ in this present experimental tank study (Table 2). Such reduction of seasonal variations were attributed to evaporation and to homogenization that permits mixing of waters of different ages during infiltration, which relates to the hydrodynamic conditions, length of flow paths, etc. In the above studies that reported seasonal isotopic variations, the time (phase) lags of $\delta^{18}O$ and δD in the findings of Luo et al. (2014), Wu et al. (2014) and Chen and Li (2018), all in Southwest China, were less than 90 days. The time lags for the two isotopes in Beddows et al. (2016), were statistically indistinguishable at 155–165+/-25 days. Compared to the time lags in our study, i.e. 131 ± 13 to 189 ± 14 days (determined chiefly by hydraulic gradient pressure through coarse primary porosity) the shorter time lags in the Chinese studies are attributable to preferential flow through mature karst solutional fractures or conduits, and the time lags in the Canadian study to piston flow through incipient fractures in a young karst terrain where the discharge rates of nine drips in three widely separated caves displayed little individual seasonal variation.

The model and natural sites compared above are very highly contrasted – five adjoining gravel-filled tanks with differing 0.5 m covers v caves in fracture aquifers with varied tree flow, litter, soil and epikarst cover. It is surprising, therefore, that the conservation of the $\delta^{18}O$ and δD seasonal signals could be quite similar in their magnitude. This underscores the controlling role that types of cover and the efficacy of evapotranspiration processes in them play in determining the amount and range of environmental information that is carried to recipient speleothems beneath them. However, given the innumerable, diverse pathways that can be randomly combined by matrix, fracture and conduit flow in natural karst aquifers (which are not modelled by our study), types of pathways need to be considered as well as types of land cover when investigating the seasonal variations of $\delta^{18}O$ and δD in groundwaters.

6. CONCLUSIONS

We have discussed $\delta^{18}O$ and δD in the precipitation and groundwater in five simulated watersheds with different land covers over the three hydrological years from November 2015 to November 2018 at Puding, SW China, a subtropical monsoon climatic region.

All of the groundwater $\delta^{18}O$ and δD displayed sinusoidal cyclicity driven by the seasonal cyclicity of $\delta^{18}O$ and δD in the precipitation. $\delta^{18}O$ and δD precipitation variations were substantially damped and lagged in all recharged groundwaters, with the damping effects ranging from 56.5 ± 2.3% to 92.7 ± 0.4% for $\delta^{18}O$ and from 60.9 ± 1.9% to 93.1 ± 0.3% for δD under the different land covers. The average phase lag times between groundwater and precipitation ranged from 131 ± 13 to 189 ± 14 days. The differences in damping effects and phase lag times in the soil-covered lands are not statistically significant from each other but do differ significantly from the bare rock land, which reveals the importance of soil cover in damping O and H isotopic seasonal variations and extending the time lags in groundwaters.

When we shifted the $\delta^{18}O$ and δD groundwater discharge records back in time by subtracting the phase lag periods, it was found that both the seasonal and inter-annual variations of $\delta^{18}O$ and δD in precipitation could be conserved under the different land covers. The inter-annual variations of comparative enrichment or depletion in all of the groundwater $\delta^{18}O$ and δD in different seasons are not simply controlled by the volumes of rainfall but by the amount-weighted isotopic input in that precipitation. Further, the signal strengths of seasonal and inter-annual $\delta^{18}O$ and δD variations in the precipitation that are conserved in groundwaters varies with land cover, the strongest conservation occurring under bare rock, with lesser, statistically inseparable, conservation in the four soil-covered tanks. It should be noted that in climates where there is only a small range of monthly mean temperatures and of the $\delta^{18}O$ and δD isotopic signals in the precipitation, soil cover can readily weaken the strength of the seasonal and inter-annual signals (as happened in the November 2016-November 2017 year at Shawan) rendering them difficult to detect in speleothems or other terrestrial carbonate precipitates. These findings may help to guide researchers to choose samples for well-preserved rainfall isotopic seasonality (e.g. in drip waters or stalagmite samples) for better high-resolution paleoclimate findings in the future.

Declaration of Competing Interest

The authors declare that they have no known competing financial interests or personal relationships that could have appeared to influence the work reported in this paper.

ACKNOWLEDGEMENTS

This work was supported by the Strategic Priority Research Program of Chinese Academy of Sciences (Grant No. XDB 40020000), the National Natural Science Foundation of China

(U1612441, 41921004 and 41673136) and the Guizhou Science and Technology Supporting Plan (No. 2020-4Y013).

APPENDIX A. SUPPLEMENTARY DATA

Supplementary data to this article can be found online at https://doi.org/10.1016/j.gca.2020.06.032.

REFERENCES

Beddows P. A., Mandić M., Ford D. C. and Schwarcz H. P. (2016) Oxygen and hydrogen isotopic variations between adjacent drips in three caves at increasing elevation in a temperate coastal rainforest, Vancouver Island, Canada. *Geochim. Cosmochim. Acta* **172**, 370–386.

Belli R., Frisia S., Borsato A., Drysdale R., Hellstrom J., Zhao J. and Spötl C. (2013) Regional climate variability and ecosystem responses to the last deglaciation in the northern hemisphere from stable isotope data and calcite fabrics in two northern Adriatic stalagmites. *Quat. Sci. Rev.* **72**, 146–158.

Bradley C., Baker A., Jex C. N. and Leng M. J. (2010) Hydrological uncertainties in the modelling of cave drip-water $\delta^{18}O$ and the implications for stalagmite palaeoclimate reconstructions. *Quat. Sci. Rev.* **29**, 2201–2214.

Chen B., Yang R., Liu Z., Sun H., Yan H., Zeng Q., Zeng S., Zeng C. and Zhao M. (2017) Coupled control of land uses and aquatic biological processes on the diurnal hydrochemical variations in the five ponds at the Shawan Karst Test Site, China: Implications for the carbonate weathering-related carbon sink. *Chem. Geol.* **456**, 58–71.

Chen C. and Li T. (2018) Geochemical characteristics of cave drip water respond to ENSO based on a 6-year monitoring work in Yangkou Cave, Southwest China. *J. Hydrol.* **561**, 896–907.

Clark I. D. and Fritz P. (1997) *Environmental Isotopes in Hydrogeology*. Lewis, Boca Ration.

Comas-Bru L. and McDermott F. (2015) Data-model comparison of soil-water $\delta^{18}O$ at a temperate site in N. Spain with implications for interpreting speleothem $\delta^{18}O$. *J. Hydrol.* **530**, 216–224.

Craig H. (1961) Isotopic variations in meteoric waters. *Science* **133**, 1702–1703.

Dansgaard W. (1953) The abundance of O^{18} in atmospheric water and water vapour. *Tellus* **5**, 461–469.

Dansgaard W. (1964) Stable isotopes in precipitation. *Tellus* **16**, 436–468.

Duan W., Ruan J., Luo W., Li T., Tian L., Zeng G., Zhang D., Bai Y., Li J., Tao T., Zhang P., Baker A. and Tan M. (2016) The transfer of seasonal isotopic variability between precipitation and drip water at eight caves in the monsoon regions of China. *Geochim. Cosmochim. Acta* **183**, 250–266.

Eichinger L., Merkel B., Nemeth G., Salvamoser J., Stichler W. and Udluft P. (1984) *Seepage velocity determinations in unsaturated quaternary gravel*. Recent investigations in the zone of aeration, Symposium proceedings, Munich, pp. 303–313.

Fairchild I. J., Smith C. L., Baker A., Fuller L., Spötl C., Mattey D. and McDermott F. (2006) Modification and preservation of environmental signals in speleothems. *Earth-Sci. Rev.* **75**, 105–153.

Fairchild I. J. and Baker A. (2012) *Speleothem Science: From Process to Past Environments*. Wiley-Blackwell, Chichester, p. 432.

Frappier A. B., Sahagian D., Carpenter S. J., González L. A. and Frappier B. R. (2007) Stalagmite stable isotope record of recent tropical cyclone events. *Geology* **35**, 111–114.

Genty D., Labuhn I., Hoffmann G., Danis P. A., Mestre O., Bourges F., Wainer K., Massault M., Van Exter S., Re´gnier E., Orengo Ph. and Falourd S. (2014) Rainfall and cave water isotopic relationships in two South-France sites. *Geochim. Cosmochim. Acta* **131**, 323–343.

Hu Y., Liu Z., Zhao M., Zeng Q., Zeng C., Chen B., Chen C., He H., Cai X., Ou Y. and Chen J. (2018) Using deuterium excess, precipitation and runoff data to determine evaporation and transpiration: A case study from the Shawan Test Site, Puding, Guizhou, China. *Geochim. Cosmochim. Acta* **242**, 21–33.

Jones M. D., Dee S., Anderson L., Baker A., Bowen G. and Noone D. C. (2016) Water isotope systematics: improving our palaeoclimate interpretations. *Quat. Sci. Rev.* **131**, 243–249.

Kendall C. and McDonnell J. J. (2012) *Isotope tracers in catchment hydrology*. Elsevier.

Kirchner J. W. (2016) Aggregation in environmental systems–Part 1: Seasonal tracer cycles quantify young water fractions, but not mean transit times, in spatially heterogeneous catchments. *Hydrol. Earth Syst. Sci.* **20**, 279–297.

Kolodny Y., Bar-Matthews M., Ayalon A. and McKeegan K. D. (2003) A high spatial resolution $\delta^{18}O$ profile of a speleothem using an ion-microprobe. *Chem. Geol.* **197**, 21–28.

Lawrence J. R., Gedzelman S. D., White J. W., Smiley D. and Lazov P. (1982) Storm trajectories in eastern US D/H isotopic composition of precipitation. *Nature* **296**, 638.

Lis G., Wassenaar L. I. and Hendry M. J. (2008) High-precision laser spectroscopy D/H and $^{18}O/^{16}O$ measurements of microliter natural water samples. *Anal. Chem.* **80**, 287–293.

Liu J., Song X., Yuan G., Sun X. and Yang L. (2014) Stable isotopic compositions of precipitation in China. *Tellus B.* **66**, 22567.

Luo W., Wang S., Zeng G., Zhu X. and Liu W. (2014) Daily response of drip water isotopes to precipitation in Liangfeng Cave, Guizhou Province, SW China. *Quat. Int.* **349**, 153–158.

Maloszewski P., Rauert W., Stichler W. and Hermann A. (1983) Application of flow models in an alpine catchment area using tritium and deuterium data. *J. Hydrol.* **66**, 319–330.

Markowska M., Baker A., Andersen M. S., Jex C. N., Cuthbert M. O., Rau G. C., Graham P. W., Rutlidge H., Mariethoz G., Marjo C. E., Treble P. C. and Edwards N. (2016) Semi-arid zone caves: Evaporation and hydrological controls on $\delta^{18}O$ drip water composition and implications for speleothem paleoclimate reconstructions. *Quat. Sci. Rev.* **131**, 285–301.

McDermott F., Mattey D. P. and Hawkesworth C. (2001) Centennial-scale Holocene climate variability revealed by a high-resolution speleothem $\delta^{18}O$ record from SW Ireland. *Science* **294**, 1328–1331.

Mueller M. H., Alaoui A., Kuells C., Leistert H., Meusburger K., Stumpp C., Weiler M. and Alewell C. (2014) Tracking water pathways in steep hillslopes by $\delta^{18}O$ depth profiles of soil water. *J. Hydrol.* **519**, 340–352.

Raymond P. A., Oh N. H., Turner R. E. and Broussard W. (2008) Anthropogenically enhanced fluxes of water and carbon from the Mississippi River. *Nature* **451**, 449.

Reddy M. M., Schuster P., Kendall C. and Reddy M. B. (2006) Characterization of surface and ground water $\delta^{18}O$ seasonal variation and its use for estimating groundwater residence times. *Hydrol. Process.* **20**, 1753–1772.

Rozanski K., Araguás-Araguás L. and Gonfiantini R. (1993) Isotopic patterns in modern global precipitation. In *Climate Change in Continental Isotopic Records. Geophysical Monograph*, vol. 78 (eds. P. K. Swart, K. C. Lohmann, J. McKenzie and S. Savin). Amer. Geophys. Union, Washington DC 20009, USA, pp. 1–36.

Serefiddin F., Schwarcz H. P., Ford D. C. and Baldwin S. (2004) Late Pleistocene paleoclimate in the Black Hills of South

Dakota from isotope records in speleothems. *Palaeogeogr. Palaeoclimatol. Palaeoecol.* **203**, 1–17.

Sinha A., Kathayat G., Weiss H., Li H., Cheng H., Reuter J., Schneider A. W., Berkelhammer M., Adali S. F., Stott L. D. and Edwards R. L. (2019) Role of climate in the rise and fall of the Neo-Assyrian Empire. *Sci. adv.* **5**, eaax6656.

Soubiès F., Seidel A., Mangin A., Genty D., Ronchail J., Plagnes V., Hirooka S. and Santos R. (2005) A fifty-year climatic signal in three Holocene stalagmite records from Mato Grosso, Brazil. *Quat. Int.* **135**, 115–129.

Stewart M. K. and McDonnell J. J. (1991) Modeling base flow soil water residence times from deuterium concentrations. *Water Resour. Res.* **27**, 2681–2693.

Tang K. and Feng X. (2001) The effect of soil hydrology on the oxygen and hydrogen isotopic compositions of plants' source water. *Earth Planet. Sci. Lett.* **185**, 355–367.

Treble P. C., Chappell J., Gagan M. K., McKeegan K. D. and Harrison T. M. (2005) In situ measurement of seasonal $\delta^{18}O$ variations and analysis of isotopic trends in a modern speleothem from southwest Australia. *Earth Planet. Sci. Lett.* **233**, 17–32.

Wackerbarth A., Langebroek P., Werner M., Lohmann G., Riechelmann S., Borsato A. and Mangini A. (2012) Simulated oxygen isotopes in cave drip water and speleothem calcite in European caves. *Clim. Past* **8**, 1781–1799.

Wang Y. J., Cheng H., Edwards R. L., He Y., Kong X., An Z., Wu J., Kelly M. J., Dykoski C. A. and Li X. (2005) The Holocene Asian Monsoon: links to solar changes and North Atlantic climate. *Science* **308**, 854–857.

White J. W. and Gedzelman S. D. (1984) The isotopic composition of atmospheric water vapor and the concurrent meteorological conditions. *J. Geophys. Res.* **89**, 4937–4939.

Wu X., Zhu X., Pan M. and Zhang M. (2014) Seasonal variability of oxygen and hydrogen stable isotopes in precipitation and cave drip water at Guilin, southwest China. *Environ. Earth Sci.* **72**, 3183–3191.

Yadava M. G., Ramesh R. and Pant G. B. (2004) Past monsoon variations in peninsular India recorded in a 331-year old speleothem. *The Holocene* **14**, 517–524.

Yang R., Liu Z., Zeng C. and Zhao M. (2012) Response of epikarst hydrochemical changes to soil CO_2 and weather conditions at Chenqi, Puding, SW China. *J. Hydrol.* **468**, 151–158.

Yonge C., Ford D., Gray J. and Schwarcz H. (1985) Stable isotope studies of cave seepage water. *Chem. Geol.* **58**, 97–105.

Yurtsever Y. and Gat J. R. (1981) Atmospheric waters. In *Stable Isotope Hydrology: Deuterium and Oxygen-18 in the Water Cycle. Technical Report Serial No. 210* (eds. J. R. Gat and R. Gonfiantini). International Atomic Energy Agency, Vienna, pp. 103–139.

Zeng C. and Liu Z. (2013) Ideas of construction of simulation test field of karst water and carbon fluxes. *Resour. Environ. Engineer.* **27**, 196–200 (in Chinese with English abstract).

Zeng C., Liu Z., Zhao M. and Yang R. (2016) Hydrologically-driven variations in the karst-related carbon sink fluxes: Insights from high-resolution monitoring of three karst catchments in Southwest China. *J. Hydrol.* **533**, 74–90.

Zeng Q., Liu Z., Chen B., Hu Y., Zeng S., Zeng C., Yang R., He H., Zhu H., Cai X., Chen J. and Ou Y. (2017) Carbonate weathering-related carbon sink fluxes under different land uses: A case study from the Shawan Simulation Test Site, Puding, Southwest China. *Chem. Geol.* **474**, 63–80.

Zhang L., Dawes W. R. and Walker G. R. (2001) Response of mean annual evapotranspiration to vegetation changes at catchment scale. *Water Resour. Res.* **37**, 701–708.

Zhang X., Liu J., Sun W., Huang Y. and Zhang J. (2007) Relations between oxygen stable isotopic ratios in precipitation and relevant meteorological factors in southwest China. *Sci. China-earth Sci.* **50**(4), 571–581.

Zhao M., Zeng C., Liu Z. and Wang S. (2010) Effect of different land use/land cover on karst hydrogeochemistry: a paired catchment study of Chenqi and Dengzhanhe, Puding, Guizhou, SW China. *J. Hydrol.* **388**, 121–130.

Zhao M., Hu Y., Zeng C., Liu Z., Yang R. and Chen B. (2018) Effects of land cover on variations in stable hydrogen and oxygen isotopes in karst groundwater: A comparative study of three karst catchments in Guizhou Province, Southwest China. *J. Hydrol.* **565**, 374–385.

Zhu H., Zeng C., Liu Z., Zeng Q. and Li L. (2015) Karst-related carbon sink flux variations caused by land use changes: an example from the Puding karst test site in Guizhou. *Hydrogeol. Engineer. Geol.* **42**, 120–125 (in Chinese with English abstract).

Associate editor: F. McDermott